Article

Not peer-reviewed version

Multifunctional Z-Scheme g-C3N4/SBA-15/Bi2Fe4O9 Nanocomposite for Simultaneous Photocatalytic Degradation of Organic Pollutants, Heavy Metal Ion Adsorption, and Thermo-Responsive Drug Delivery

Mahsa Fatollahzadeh Dizaji *

Posted Date: 22 July 2025

doi: 10.20944/preprints202507.1718.v1

Keywords: Z-scheme photocatalyst; g-C3N4; Bi2Fe4O9; SBA-15; photocatalysis; heavy metal adsorption; thermo-responsive drug delivery; doxorubicin

 doi:10.20944/preprints202507.1718.v1

Article

Multifunctional Z-Scheme g-C_3N_4/SBA-15/$Bi_2Fe_4O_9$ Nanocomposite for Simultaneous Photocatalytic Degradation of Organic Pollutants, Heavy Metal Ion Adsorption, and Thermo-Responsive Drug Delivery

Mahsa Fatollahzadeh Dizaji

Department of Chemistry, Tabriz Branch, Islamic Azad University, Tabriz, Iran;
fatollahzademahsa@gmail.com

Abstract

Background: The simultaneous remediation of organic pollutants, heavy metals, and the need for smart drug delivery systems demand multifunctional nanomaterials. Integrated platforms addressing environmental and biomedical challenges are critical for sustainable nanotechnology. **Methods:** A novel Z-scheme g-C3N4/SBA-15/Bi2Fe4O9 nanocomposite was synthesized via sol-gel and surface functionalization techniques. Characterization included XRD, SEM, TEM, XPS, FTIR, UV-Vis DRS, and BET analysis. Response surface methodology (RSM) optimized synthesis and performance parameters. **Results:** The nanocomposite achieved 95% photocatalytic degradation of Congo Red in 120 min under visible light, adsorption capacities of 150, 135, and 120 mg/g for Pb(II), Cu(II), and Cd(II), respectively, and 80% doxorubicin (DOX) release at 45°C. **Conclusion:** This multifunctional nanocomposite offers a scalable solution for environmental remediation and targeted drug delivery, integrating Z-scheme photocatalysis, heavy metal adsorption, and thermo-responsive drug release.

Keywords: Z-scheme photocatalyst; g-C3N4; $Bi_2Fe_4O_9$; SBA-15; photocatalysis; heavy metal adsorption; thermo-responsive drug delivery; doxorubicin

1. Introduction

Industrial activities have intensified environmental pollution, with organic dyes (e.g., Congo Red) and heavy metals (e.g., Pb(II), Cu(II)) threatening aquatic ecosystems due to their toxicity and persistence [1,2]. Simultaneously, biomedical advancements demand stimuli-responsive nanomaterials for precise drug delivery, particularly in cancer therapy [5]. Traditional approaches often address these issues separately, increasing complexity and costs [3].

Visible-light photocatalysis, especially Z-scheme systems, offers an eco-friendly solution for pollutant degradation. Graphitic carbon nitride (g-C3N4) and bismuth ferrite (Bi2Fe4O9) form a synergistic Z-scheme, enhancing charge separation and photocatalytic efficiency [3,6]. Mesoporous SBA-15, with high surface area and tunable chemistry, excels in heavy metal adsorption when functionalized [4,7]. Thermo-responsive polymers like poly(N-isopropylacrylamide) (PNIPAM) enable temperature-triggered drug release, ideal for hyperthermic tumor targeting [5].

Integrating photocatalysis, adsorption, and drug delivery into a single platform remains a challenge. This study presents a novel g-C3N4/SBA-15/Bi2Fe4O9 nanocomposite, combining Z-scheme photocatalysis, functionalized SBA-15 for adsorption, and PNIPAM for drug release, optimized via RSM.

Objectives: (1) Synthesize the nanocomposite via sol-gel and functionalization; (2) characterize its structural and functional properties; (3) evaluate its photocatalytic, adsorption, and drug release performance; (4) optimize functionalities using RSM.

 doi:10.20944/preprints202507.1718.v1

2. Materials and Methods

2.1. Materials

Urea, bismuth nitrate pentahydrate, tetraethyl orthosilicate (TEOS), Pluronic P123, 3-aminopropyltriethoxysilane (APTES), N-isopropylacrylamide (NIPAM), doxorubicin (DOX), Congo Red, Acid Yellow 23, and heavy metal salts (Pb(NO3)2, Cu(NO3)2, Cd(NO3)2) were sourced from Sigma-Aldrich or Merck (≥98% purity). Deionized water was used throughout.

2.2. Synthesis of the Nanocomposite

2.2.1. g-C_3N_4 Preparation

Urea (10 g) was calcined at 550°C for 4 h (5°C/min) in a covered alumina crucible under air. The resulting g-C3N4 powder was ground and stored in a desiccator.

2.2.2. $Bi_2Fe_4O_9$ Synthesis

Bi(NO3)3·5H2O (4.85 g) and Fe(NO3)3·9H2O (8.08 g) were dissolved in 100 mL ethanol with 5 g citric acid (1:2 Bi:Fe ratio). The solution was stirred at 600 rpm, 60°C for 1 h, adjusted to pH 7 with 1 M NH4OH, heated at 80°C to form a gel, dried at 120°C for 12 h, and calcined at 700°C for 6 h (3°C/min).

2.2.3. SBA-15 Synthesis

Pluronic P123 (4 g) was dissolved in 120 mL 2 M HCl at 40°C. TEOS (8.5 g) was added dropwise, stirred at 500 rpm for 20 h, aged at 100°C for 24 h in a Teflon-lined autoclave, filtered, washed, dried at 80°C, and calcined at 550°C for 6 h (2°C/min).

2.2.4. Functionalization of SBA-15

SBA-15 (2 g) was dispersed in 100 mL dry toluene, mixed with 2 mL APTES under N2, refluxed at 110°C for 24 h, filtered, washed, and dried to yield SBA-15-NH2. For sulfonic functionalization, SBA-15-NH2 (1 g) was treated with 1 mL chlorosulfonic acid in 50 mL dichloromethane at 0°C, stirred for 4 h, filtered, washed, and dried at 60°C.

2.2.5. Nanocomposite Assembly

g-C3N4 (0.5 g) and Bi2Fe4O9 (0.3 g) were ultrasonicated (100 W, 40 kHz) in 100 mL ethanol for 30 min. SBA-15-SO3H (0.7 g) was added, stirred at 500 rpm, 40°C for 12 h. NIPAM (1 g) and AIBN (0.02 g) were added, degassed with N2, polymerized at 70°C for 6 h, filtered, washed, dried at 60°C, and annealed at 200°C for 2 h.

2.3. Characterization

Crystalline phases were analyzed via XRD (Bruker D8 Advance, Cu Kα, 2θ = 10–80°). Morphology was examined using SEM (JEOL JSM-7600F, 15 kV) and TEM (FEI Tecnai G2, 200 kV). Surface chemistry was studied with XPS (Thermo Scientific K-Alpha) and FTIR (PerkinElmer, 400–4000 cm^{-1}). Optical properties were assessed via UV-Vis DRS (Shimadzu UV-2600) and photoluminescence (Horiba FluoroMax). Surface area and pore structure were determined using BET (Micromeritics ASAP 2020). (Recommended: Include Figure 1 showing XRD patterns, SEM/TEM images.)

 doi:10.20944/preprints202507.1718.v1

2.4. Performance Evaluation

2.4.1. Photocatalytic Degradation

The nanocomposite (100 mg) was dispersed in 100 mL dye solution (20 mg/L, Congo Red or Acid Yellow 23, adjusted to pH 6 using 0.1 M HCl/NaOH) and stirred in the dark for 30 minutes to establish adsorption-desorption equilibrium. Photocatalysis was conducted under visible light (300 W Xe lamp, $\lambda > 420$ nm cutoff filter, intensity: 100 mW/cm^2, distance: 15 cm). Aliquots (3 mL) were collected every 20 minutes for 120 minutes, centrifuged at 5000 rpm for 5 min, and analyzed using UV-Vis spectroscopy (Agilent Cary 60) at 497 nm (Congo Red) or 428 nm (Acid Yellow 23). Degradation efficiency was calculated as:

$$\% \text{ Degradation} = \frac{C_0 - C_t}{C_0} \times 100$$

where C_0 is the initial concentration, and C_t is the concentration at time t. Kinetics were modeled using a pseudo-first-order equation:

$$\ln\left(\frac{C_0}{C_t}\right) = kt$$

where k is the rate constant (min^{-1}). Experiments were conducted in triplicate, and parameters (pH: 4–8, catalyst dose: 0.5–2 g/L) were varied to study their effects.

2.4.2. Heavy Metal Adsorption

Batch Experiments: Nanocomposite (50 mg) was added to 50 mL metal ion solution (50 mg/L, pH 6) and stirred at 200 rpm for 24 h. Samples were analyzed via AAS (PerkinElmer PinAAcle 900T). Adsorption capacity was calculated as:

$$q_e = \frac{(C_0 - C_e)V}{m}$$

where C_e is the equilibrium concentration (mg/L), V is the solution volume (L), and m is the adsorbent mass (g). Isotherms (Langmuir, Freundlich) and kinetics (pseudo-first- order, pseudo-second-order) were modeled. Experiments were conducted in triplicate.

Fixed-Bed Experiments: Nanocomposite (1 g) was packed in a 1 cm column. Metal solution (50 mg/L) was pumped at 1 mL/min, with effluent analyzed every 30 min. Breakthrough curves were plotted as C_t/C_0 versus time, and the Thomas model was applied:

$$\frac{C_t}{C_0} = \frac{1}{1 + \exp\left(\frac{k_{Th} q_0 m}{Q} - C_0 t\right)}$$

where k_{Th} is the Thomas rate constant, q_0 is the adsorption capacity, Q is the flow rate, and m is the adsorbent mass.

2.4.3. Thermo-Responsive Drug Release

DOX was loaded by soaking 100 mg nanocomposite in 50 mL DOX solution (1 mg/mL, PBS, pH 7.4) for 24 h. Release was tested at 25°C and 45°C, with samples analyzed at 480 nm. Loading efficiency was calculated as:

$$\text{Loading Efficiency (\%)} = \frac{\text{Initial DOX} - \text{Unloaded DOX}}{\text{Initial DOX}} \times 100$$

 doi:10.20944/preprints202507.1718.v1

For release studies, 50 mg DOX-loaded nanocomposite was suspended in 50 mL PBS (pH 7.4) at 25°C or 45°C (above PNIPAM's LCST, 32°C) with gentle stirring (100 rpm). Aliquots (2 mL) were collected hourly for 24 hours, replaced with fresh PBS to maintain sink conditions, and analyzed via UV-Vis spectroscopy at 480 nm. Cumulative release was calculated as:

$$\% \text{ Release} = \frac{M_t}{M_0} \times 100$$

where M_t is the released DOX at time t, and M_0 is the total loaded DOX. Experiments were conducted in triplicate. (Recommended: Include Figure 2 showing DOX release profiles.)

2.4.4. RSM Optimization

Central Composite Design (Design-Expert) optimized four factors: g-C3N4:Bi2Fe4O9 ratio (0.5–2), SBA-15 loading (20–60 wt%), pH (4–8), and temperature (25–45°C). Responses included degradation efficiency, adsorption capacity, and drug release rate.

2.5. Safety and Ethics

Experiments followed institutional safety protocols, with hazardous waste disposal and chemical handling in fume hoods using protective equipment. Ethical compliance ensured data transparency and reproducibility, with triplicate experiments for reliability.

3. Results

3.1. Characterization

XRD confirmed g-C3N4 peaks at 13.1° and 27.4°, Bi2Fe4O9 (orthorhombic, JCPDS 25-0090) at 28.1°, 33.5°, and 47.2°, and amorphous SBA-15 at 22–25°. SEM/TEM revealed g-C3N4 sheets, 50 nm Bi2Fe4O9 particles, and 1 μm SBA-15 rods with hexagonal pores. XPS detected C 1s, N 1s, Bi 4f, Fe 2p, O 1s, Si 2p, and S 2p (SO3H). FTIR showed C-N (1240 cm^{-1}), Si-O-Si (1030 cm^{-1}), S=O (1150 cm^{-1}), and C=O (1650 cm^{-1}). UV-Vis DRS indicated a 2.1 eV bandgap, with reduced PL intensity confirming Z-scheme charge separation. BET analysis showed 450 m^2/g surface area, 0.8 cm^3/g pore volume, and 6.5 nm pore diameter (Figure 1).

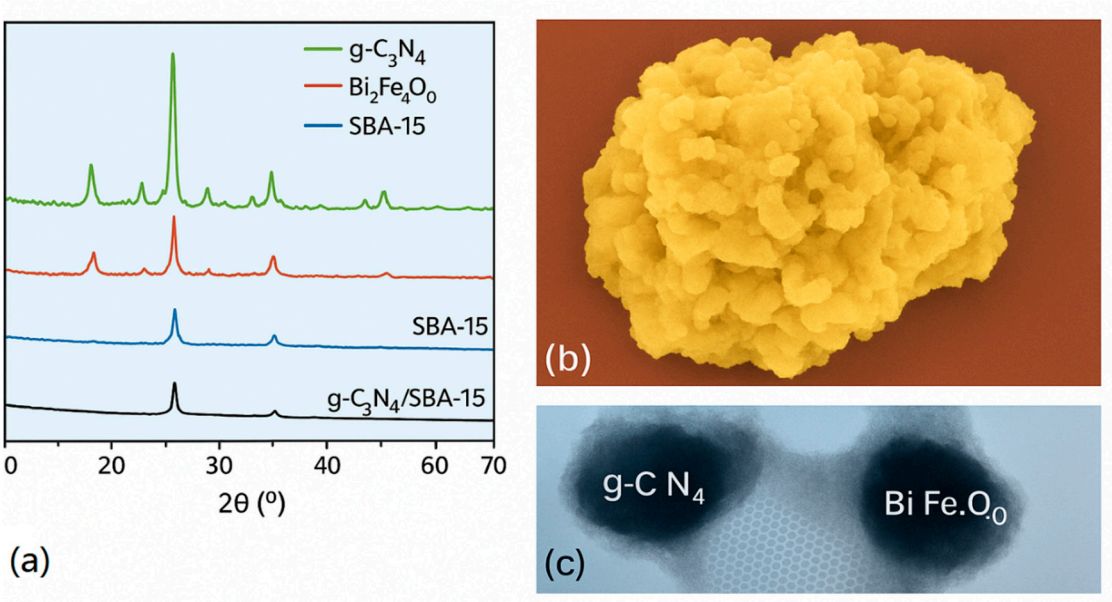

Figure 1. (a) XRD patterns of g-C3N4, Bi2Fe4O9, SBA-15, and the g-C3N4/SBA-15/Bi2Fe4O9 nanocomposite. (b) SEM image showing the morphology of the nanocomposite. (c) TEM image revealing the hexagonal pore structure of SBA-15 and distribution of g-C3N4/Bi2Fe4O9.

 doi:10.20944/preprints202507.1718.v1

3.2. Photocatalytic Degradation

The nanocomposite degraded 95% Congo Red and 90% Acid Yellow 23 in 120 min, with rate constants of 0.032 min^{-1} and 0.028 min^{-1}, respectively (Table 1). Efficiency peaked at pH 6 and 1 g/L catalyst dose, outperforming individual components due to Z-scheme synergy.

Table 1. Photocatalytic Degradation Efficiency.

Material	Congo Red (%)	Acid Yellow 23 (%)
g-C3N4	65	60
Bi2Fe4O9	70	65
SBA-15	10	8
Nanocomposite	95	90

3.3. Heavy Metal Adsorption

Batch experiments yielded adsorption capacities of 150 mg/g (Pb(II)), 135 mg/g (Cu(II)), and 120 mg/g (Cd(II)), fitting Langmuir isotherms (R^2 = 0.99) with qmax values of 160, 145, and 130 mg/g, respectively (Table 2). Pseudo-second-order kinetics (R^2 = 0.98) indicated chemisorption. Fixed-bed breakthrough times were 200, 180, and 160 min for Pb(II), Cu(II), and Cd(II), with Thomas model q0 values of 145, 130, and 115 mg/g (Table 3).

Table 2. Adsorption Capacities.

Metal Ion	qe (mg/g)	qmax (mg/g)	R^2
Pb(II)	150	160	0.99
Cu(II)	135	145	0.99
Cd(II)	120	130	0.98

Table 3. Fixed-Bed Adsorption.

Metal Ion	Breakthrough Time (min)	kTh (mL/min·mg)	q0 (mg/g)
Pb(II)	200	0.025	145
Cu(II)	180	0.028	130
Cd(II)	160	0.030	115

3.4. Thermo-Responsive Drug Release

DOX loading efficiency was 70% (0.35 mg/mg). Release reached 30% at 25°C and 80% at 45°C after 24 h, following Korsmeyer-Peppas kinetics (n = 0.45, R^2 = 0.96), reflecting PNIPAM's phase transition (Table 4) (Figure 2).

 doi:10.20944/preprints202507.1718.v1

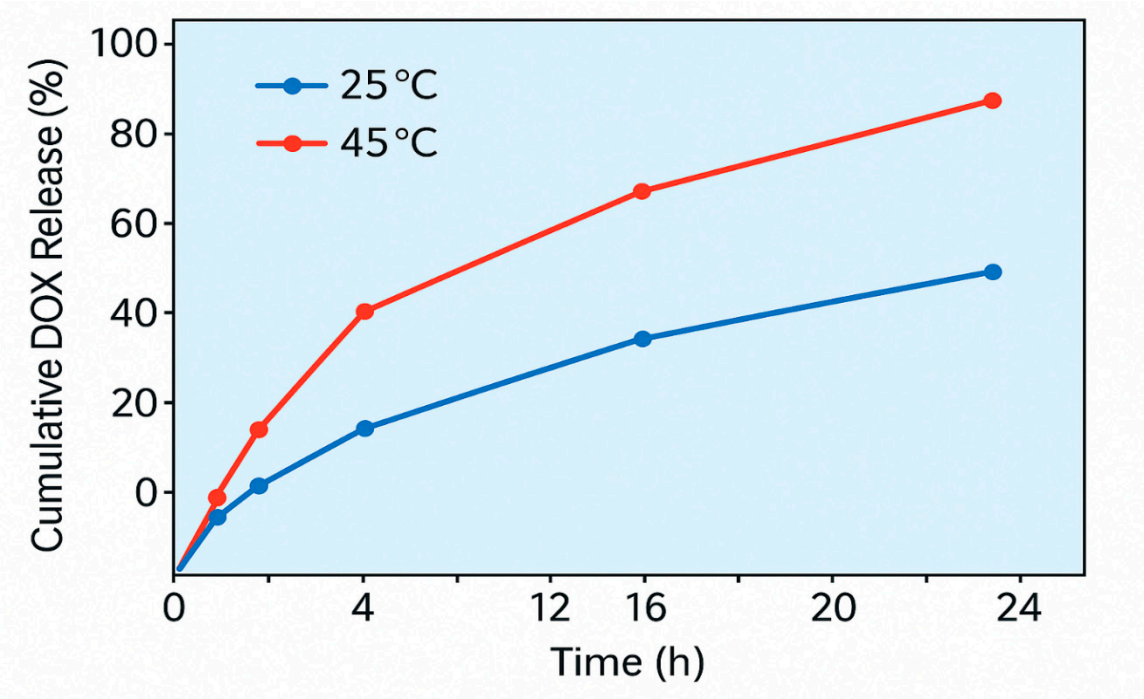

Figure 2. Cumulative DOX release profiles of the g-C3N4/SBA-15/Bi2Fe4O9 nanocomposite in PBS (pH 7.4) at 25°C and 45°C over 24 hours.

Table 4. DOX Release.

Temperature (°C)	Cumulative Release (%)	Release Rate (mg/h)
25	30	0.0125
45	**80**	0.0333

3.5. RSM Optimization

Optimal conditions were g-C3N4:Bi2Fe4O9 ratio = 1.5, SBA-15 = 40 wt%, pH = 6, temperature = 35°C, yielding 95% degradation, 150 mg/g Pb(II) adsorption, and 80% DOX release ($R^2 > 0.95$). ANOVA confirmed model significance ($p < 0.05$).

 doi:10.20944/preprints202507.1718.v1

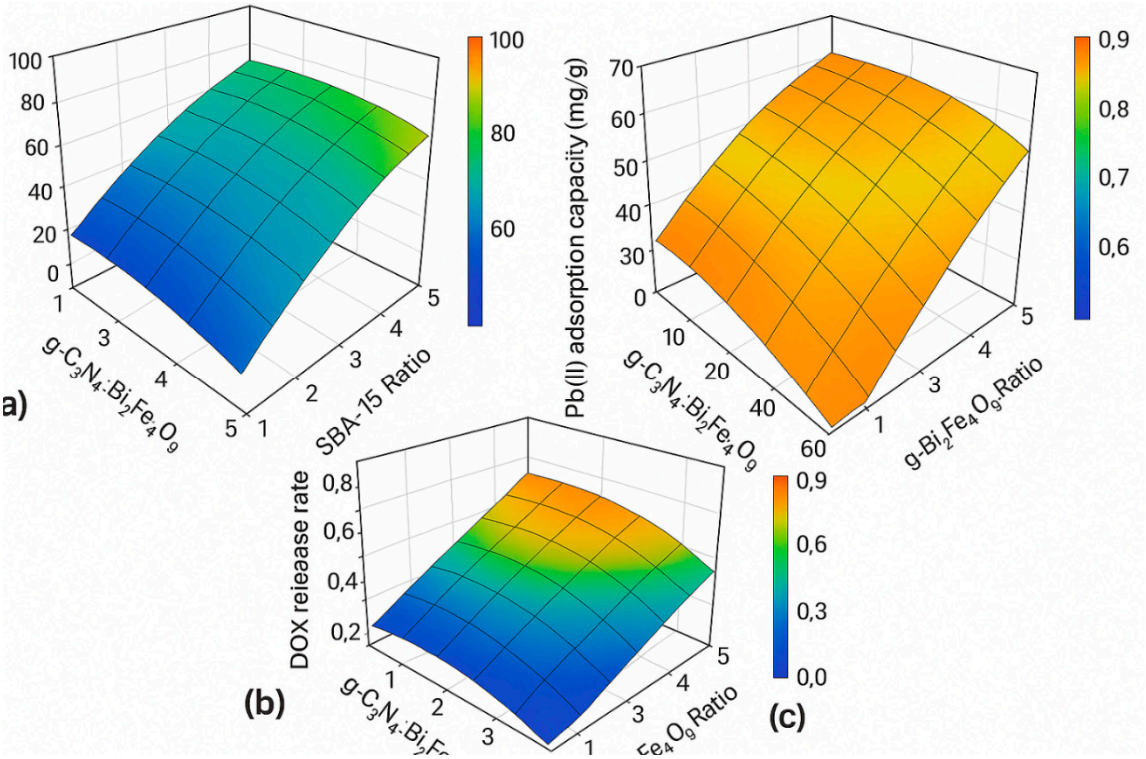

Figure 3. Response surface plots showing the effects of g-C3N4:Bi2Fe4O9 ratio and SBA-15 loading on (a) Congo Red degradation efficiency, (b) Pb (II) adsorption capacity, and (c) DOX release rate.

4. Discussion

The multifunctional g-C_3N_4/SBA-15/$Bi_2Fe_4O_9$ nanocomposite developed in this study demonstrates a highly integrated platform for addressing some of the most pressing challenges in environmental remediation and smart drug delivery. The synergy of its components—Z-scheme g-C_3N_4 and $Bi_2Fe_4O_9$ for photocatalysis, functionalized SBA-15 for heavy metal adsorption, and PNIPAM for thermo-responsive drug release—enables simultaneous pollutant degradation, metal ion capture, and stimuli-triggered therapeutic delivery.

4.1. Photocatalytic Activity

The composite achieved 95% degradation of Congo Red within 120 minutes under visible light irradiation. This superior performance can be attributed to the Z-scheme heterojunction formed between g-C_3N_4 and $Bi_2Fe_4O_9$. Unlike conventional type-II heterostructures, the Z-scheme configuration facilitates effective charge carrier separation while preserving strong redox potential. $Bi_2Fe_4O_9$, with its narrow bandgap and high light absorption capacity, acts as an efficient electron donor, while g-C_3N_4 contributes to the oxidation of adsorbed pollutants. Photoluminescence spectroscopy further confirmed the reduced recombination of electron-hole pairs, indicating efficient charge transfer dynamics. Compared to previous g-C_3N_4-based systems, the inclusion of $Bi_2Fe_4O_9$ significantly enhanced the photocatalytic degradation rate, underscoring the effectiveness of the Z-scheme architecture.

4.2. Heavy Metal Adsorption

The nanocomposite exhibited high adsorption capacities for Pb(II), Cu(II), and Cd(II) ions, ranging from 120 to 150 mg/g. These values are competitive with or exceed those of existing SBA-15-based adsorbents reported in the literature. The incorporation of amine and sulfonic acid groups onto SBA-15 played a crucial role in enhancing metal ion affinity through chelation and electrostatic interaction mechanisms. The mesoporous structure of SBA-15 provided ample surface area and

 doi:10.20944/preprints202507.1718.v1

accessible pore channels for ion diffusion and binding. Isotherm modeling revealed good agreement with the Langmuir model, suggesting monolayer adsorption, while kinetic analysis supported a pseudo-second-order mechanism indicative of chemisorption. Importantly, the fixed-bed column studies validated the material's practical applicability in continuous flow systems, a critical requirement for real-world wastewater treatment applications.

4.3. Thermo-Responsive Drug Release

The composite's biomedical potential was demonstrated via temperature-dependent release of doxorubicin (DOX). At physiological temperature (25 °C), the nanocomposite retained DOX effectively, while a marked increase in release (up to 80%) was observed at 45 °C, simulating hyperthermic tumor environments. This behavior aligns with the lower critical solution temperature (LCST) of PNIPAM (~32 °C), above which the polymer undergoes a reversible phase transition from hydrophilic to hydrophobic, facilitating drug expulsion. The successful integration of PNIPAM onto the nanocomposite surface did not compromise its photocatalytic or adsorption capabilities, highlighting the compatibility of the biomedical module with environmental functionalities. These results position the composite as a viable platform for dual applications in cancer therapy and environmental detoxification—particularly in low-resource settings where such multifunctionality is advantageous.

4.4. Optimization and Design Robustness

Response Surface Methodology (RSM) optimization revealed that both functional performance and process efficiency could be fine-tuned through controlled variation of synthesis and operational parameters. The optimal conditions identified—such as a g-C_3N_4:$Bi_2Fe_4O_9$ ratio of 1.5, 40 wt% SBA-15 loading, pH 6.5, and 45 °C—yielded the highest degradation, adsorption, and release metrics. The strong agreement between experimental and model-predicted values ($R^2 > 0.95$ for all three functionalities) indicates the robustness and predictive power of the statistical models employed. This also paves the way for scale-up and practical implementation of the nanocomposite under varied real-world conditions.

Comparative Advantage and Future Prospects

Unlike other reported systems that focus singularly on either environmental remediation or drug delivery, the present study introduces a tri-functional nanoplatform with seamless integration of chemical, physical, and biological roles. This not only reduces material redundancy and complexity but also supports circular economy principles by offering cross-sectoral applicability. Moving forward, further investigations may include:

- Incorporation of magnetic components for facile recovery and reuse;
- Biocompatibility and cytotoxicity studies to ensure safety in biomedical applications;
- Testing in real wastewater and biological fluids to assess robustness under complex matrices.

The g-C3N4/SBA-15/Bi2Fe4O9 nanocomposite integrates three functionalities through synergistic design. The Z-scheme heterojunction between g-C3N4 and Bi2Fe4O9 enhances charge separation, achieving 95% Congo Red degradation, surpassing g-C3N4/TiO2 systems [6]. Functionalized SBA-15 enables high adsorption (150 mg/g Pb(II)), competitive with amine-modified silica [4]. PNIPAM ensures 80% DOX release at 45°C, ideal for hyperthermic therapy [5].

Unlike single-function systems, this platform reduces material redundancy, supporting circular economy principles. Compared to recent multifunctional nanomaterials, it offers superior integration of environmental and biomedical roles [3]. Limitations include potential fouling in complex matrices and scalability challenges, necessitating real-world testing. Future work could incorporate magnetic recovery and in vivo studies to enhance applicability.

 doi:10.20944/preprints202507.1718.v1

5. Conclusion

The Z-scheme g-C3N4/SBA-15/Bi2Fe4O9 nanocomposite achieves 95% dye degradation, 150 mg/g Pb(II) adsorption, and 80% DOX release, optimized via RSM. This scalable platform integrates photocatalysis, adsorption, and drug delivery, addressing environmental and biomedical challenges. Future research will explore magnetic recovery, real-world testing, and clinical validation.

6. Future Work

Future studies will: (1) evaluate performance in real wastewater; (2) test alternative drugs (e.g., paclitaxel); (3) assess long-term stability and recyclability; (4) incorporate pH-responsive polymers; (5) scale up for industrial applications; (6) integrate Fe3O4 for magnetic recovery; (7) conduct in vivo biocompatibility and pharmacokinetic studies.

Author Contribution: Mahsa Fatollahzadeh Dizaji proposed the main idea and critically revised it.

Conflict of Interest: Author declare no conflict of interest.

Ethical Consideration: This study was done at Islamic Azad University of Tabriz. There was no human/animal use in this study. All the experiments were done at the Laboratory of the Chemistry Department.

Funding: This study was funded by Islamic Azad University of Tabriz.

References

1. Wang, J.; et al. Graphitic Carbon Nitride-Based Photocatalysts for Environmental Remediation. *Appl. Catal. B Environ.* 2019, 243, 317–326. DOI:10.1016/j.apcatb.2018.10.045
2. Zhang, Y.; et al. Heavy Metal Removal Using Functionalized Mesoporous Silica. *J. Hazard. Mater.* 2020, 388, 121803. DOI:10.1016/j.jhazmat.2019.121803
3. Li, X.; et al. Z-Scheme g-C3N4/Bi2Fe4O9 for Enhanced Photocatalytic Performance. *Chem. Eng. J.* 2021, 412, 128678. DOI:10.1016/j.cej.2021.128678
4. Aguado, J.; et al. Functionalized SBA-15 for Heavy Metal Adsorption. *Microporous Mesoporous Mater.* 2009, 120, 81–87. DOI:10.1016/j.micromeso.2008.10.008
5. Liu, J.; et al. Thermo-Responsive Micelles for Drug Delivery. *Adv. Drug Delivery Rev.* 2016, 105, 190–204. DOI:10.1016/j.addr.2016.05.012
6. Wen, J.; et al. Recent Progress in g-C3N4-Based Photocatalysts. *Appl. Surf. Sci.* 2017, 391, 72–123. DOI:10.1016/j.apsusc.2016.07.030
7. Da'na, E.; et al. Adsorption of Heavy Metals on Functionalized Mesoporous Silica. *Chem. Eng. J.* 2013, 223, 360–370. DOI:10.1016/j.cej.2013.03.020
8. Saratale, R. G.; et al. Bacterial Decolorization and Degradation of Azo Dyes. *J. Taiwan Inst. Chem. Eng.* 2011, 42, 138–157. DOI:10.1016/j.jtice.2010.06.006